Geometry Based Pectoral Muscle Segmentation from MLO Mammogram Views

Saeid Asgari Taghanaki*, Yonghuai Liu, *Senior Member, IEEE,* Brandon Miles, and Ghassan Hamarneh, *Senior Member, IEEE*

***Abstract*—Computer aided diagnosis systems (CADx) play a major role in the early diagnosis of breast cancer. Extracting the breast region precisely from a mammogram is an essential component of CADx for mammography. The appearance of the pectoral muscle on medio-lateral oblique (MLO) views increases the false positive rate in CADx. Therefore, the pectoral muscle should be identified and removed from the breast region in an MLO image before further analysis. None of the previous pectoral muscle segmentation methods address all breast types based on the breast imaging-reporting and data system (BI-RADS) tissue density classes. In this paper, we deal with this deficiency by introducing a new simple yet effective method that combines geometric rules with a region growing algorithm to support the segmentation of all types of pectoral muscles (normal, convex, concave, and combinatorial). Experimental segmentation accuracy results were reported for four tissue density classes on 872 MLO images from three publicly available datasets. An average Jaccard index and Dice similarity coefficient of 0.972±0.003 and 0.985±0.001 were obtained, respectively. The mean Hausdorff distance between the contours detected by our method and the ground truth is below 5mm for all datasets. An average acceptable segmentation rate of ~95% was achieved outperforming several state-of-the-art competing methods. Excellent results were obtained even for the most challenging class of extremely dense breasts.**

***Index Terms*—Breast cancer, computer aided diagnosis, digital mammography, geometry rule-based segmentation.**

I. Introduction

FOR women from 15 to 54 years of age, breast cancer is the leading cause of death [1]. Mammography is a standard tool for the early diagnosis of breast cancer. To address the limitations of manual visual inspection for screening mammography, such as reduced sensitivity in dense breasts, misinterpreting non-cancerous lesions as cancer and vice versa, as well as to reduce time and cost, computer-aided detection/diagnosis systems (CADx) have been developed [2, 3]. One critical issue in mammogram processing for CADx is that the pectoral muscle lies posterior to the breast and has a similar density to tumor cells. As a result, the appearance of the pectoral muscle on medio-lateral oblique (MLO) views usually increases the false positive rate of CADx [4]. Although many articles have been published in the past decade on pectoral muscle segmentation and despite the fact that there are some commercially available tools, they either require human intervention or have a low accuracy rate that negatively affects the subsequent diagnosis and therapy planning. Therefore, there remains a need for developing automatic, fast, and robust mammography CADx systems [5-9]. To the best of our knowledge, we are unable to identify a CADx method that supports all types of muscles with high accuracy on all four tissue density classes defined in the breast imaging-reporting and data system (BI-RADS), introduced by the American College of Radiology [10]: 1. almost entirely fatty; 2. scattered fibro-glandular; 3. heterogeneously dense; and 4. extremely dense.

In one of the earliest studies [11], the authors defined a rectangle to isolate the pectoral muscle from a region of interest (ROI). They then attempted to remove the pectoral muscle using a modified region growing (RG) method. However, the ROI in this method continues to include a large portion of the pectoral muscle leading to erroneous segmentation of the muscle. The Hough transform and cliff detection techniques were used by Kwok et al. [12] to delineate the pectoral muscle region. However, the performance of this method deteriorates significantly when the breast tissue contains complex textures, which is often the case. Also, it is not justifiable to adopt a straight-line assumption (as done in [12]) since the curvature of the muscle boundary can vary.

Ferrari et al. [13] applied a multi-resolution procedure using Gabor wavelets to enhance the edge of the pectoral muscle and a method called edge-flow propagation [34] to detect relevant edges of the pectoral muscle. Although this approach addresses some weaknesses of the straight-line representation, the identified pectoral muscle may be under-segmented when the glandular tissue obscures the muscle. Another approach that is based on adaptive pyramids and minimum spanning trees was introduced by Ma et al. [14]. This method obtained unsatisfactory results for multi-layer pectoral muscles. In Raba et al. [15], the authors combined RG with morphological operators to identify the muscle. However, in dense breasts, the muscle region may be over/under-segmented due to the nature of the intensity threshold estimation based RG which they used. Furthermore, their method needs to specify the RG

S. A. Taghanki*, B. Miles, and G. Hamarneh are with the School of Computing Science, Simon Fraser University, Canada ({sasgarit, bmiles, hamarneh}@sfu.ca).

Yonghuai Liu is with the Department of Computer Science, Aberystwyth University, UK (yyl@aber.ac.uk).

seed point manually. Mustra et al. [16] implemented a bit-depth reduction method in combination with wavelet decomposition for detecting the pectoral muscle. This approach obtained desirable results only on the images with a high contrast between the pectoral muscle and the surrounding tissue, but a drop in performance is evident in low contrast and small pectoral muscles.

In the work of Wang et al. [17], the authors tried to address some of the drawbacks of the methods mentioned above, such as the inability to handle various curvature types and multi-layered muscles, using a discrete time Markov chain and an active contour model. In the first steps of their method, they separated the breast into two regions of interest (two separate regions containing the pectoral muscle); however, this separation process is highly dependent on contrast. Camilus et al. [18] attempted to segment the pectoral muscle using a graph cut based region merging algorithm combined with an underlying Bezier curve shape representation. However, their results were sensitive to the order in which the regions were merged. Later, Camilus et al. [19] presented a watershed transformation-based algorithm. However, the watershed method often leads to over-segmentation, and it is cumbersome to adjust the merging criterion. Other recent works can be found in Ganesan et al. [4].

An important issue that has not been addressed in all these works is performance evaluation on the third and fourth BI-RADS tissue density classes. In these two classes, a significant part of the breast is made up of fibrous and glandular tissues, which makes the segmentation even more challenging. The risk of breast cancer increases in higher breast densities (a 4 to 6-fold increase in breast cancer risk has been reported in women with extremely dense breasts compared to those with predominantly fatty breasts [20]) hence, this issue should not be ignored. Higher densities also affect the sensitivity and accuracy of CADx, as tumors are concealed behind the higher attenuating fibro-glandular tissue areas [21]. To the best of our knowledge, we could not identify an existing method robust to all tissue density classes, brightness, multi-layer muscles, and to the size of the breast and muscle.

In this paper, a geometrical rule-based algorithm for the segmentation of the pectoral muscle is proposed. The method supports all types of pectoral muscles without any limitation on the size of the breast or muscle. Since accurate segmentation is highly dependent on finding the edge of the muscle, edge detection techniques based on color or brightness may fail when dealing with complex textures. In contrast, our proposed method is based on geometric rules instead and thus is robust to different image appearances. Since the basis of our method is not based on tissue, color, or contrast, we would expect the algorithm to have improved performance on almost all BI-RADS density categories. Nevertheless, for supporting the other types of muscles such as convex, concave, or their combination, we optimize the proposed method via a modified region growing algorithm designed to limit the region for the RG algorithm. Our method also chooses the region growing seed point automatically.

II. METHODS

The first challenge for pectoral muscle segmentation is to identify the approximate location of the pectoral muscle. The pectoral muscle and the breast should be distinguishable given their different locations and appearances in mammographic imaging. A careful observation shows that the breast is contained within a right angle triangle (this is true for MLO views; because the imaging is performed with the patient in a standing position with their breast resting on a flat surface, thus forming a right angle triangle) and the inferior region of the breast can be approximated as a circle (Fig. 1). Together, the triangle and circle form a rough geometric model of the imaged breast region. Knowing that the muscle is located posterior to the breast (Fig. 1), we fit a circle (a maximum inscribed circle, MIC, to be exact) inside the approximating triangle and localize the desired muscle region as the region located inside the triangle but above (i.e. superior to) the MIC. Fig. 1 shows that other possible geometrical shapes, e.g. maximum inscribed rectangle (MIR), square (MIS), or oval (MIO), would not be as suitable as the proposed MIC. Our method to locate the pectoral muscle consists of 3 main steps: (1) Pre-filtering and breast boundary detection; (2) Identification of the muscle location via geometric rules; and (3) Optimization of the method for convex and combinatorial muscles.

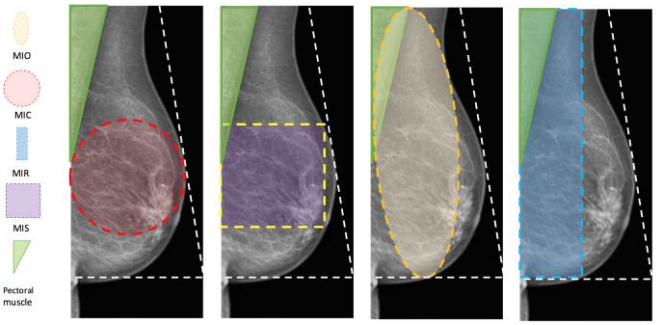

Fig. 1. Illustration of the similarity of the breast to a right angle triangle (white dashed line) and how the MIC helps identify the muscle region.

A. *Pre-filtering and breast boundary detection*

Mammograms are essentially low contrast images with inconspicuous edges. We first perform contrast-limited adaptive histogram equalization (CLAHE) [11] to the images to enhance their contrast and obtain clearer details and stronger edges. In our experiment, the CLAHE parameters have been set as follows: We defined the number of rectangular contextual regions (tiles) to be 2×2. The optimal number of tiles is dependent on the input image, and it is best determined through experimentation. The contrast factor (Cf) avoids over-saturation of the image in homogeneous areas and was limited to 0.01. The number of 'bins' for the histogram needed for the contrast enhancement transformation was set to 256. The 'uniform' mode was selected for the histogram distribution. In order to detect the breast contour, we converted the grey-scale image to a binary image with threshold t set to 0.3 (or lower) and applied the Canny edge

detector. The steps to obtain the breast contour are shown in Fig. 2.

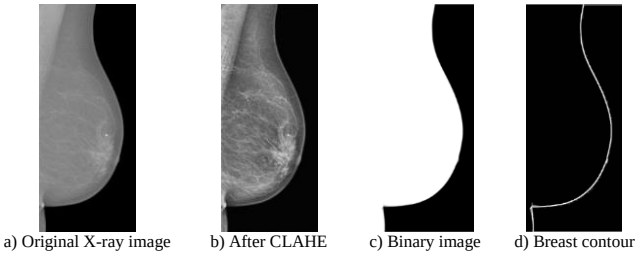

Fig. 2. The steps for detecting the contour of the breast; applying CHAHE, converting the grey image into a binary one, and the detected edge.

To set the parameters, we tested several different values e.g., the Cf parameter was changed from 0.005 to 0.015. As illustrated in Fig. 3, Cf = 0.01 produced sharper images than other values. Although it is barely palpable (visually), the edges in the images with Cf = 0.005 are not clear enough to separate the regions easily while the images with Cf = 0.015 are likely to cause miscalculation in the region growing step because the gray-level values of the muscle region will be similar to the surrounding tissue (see the areas with a dashed black oval). The threshold value for converting gray images to binary ones was varied from 0.03 to 0.15. As can be seen in Fig. 4, the value of *t* that resulted in the best contour detection is 0.03. Note that the parameters are fixed for all images.

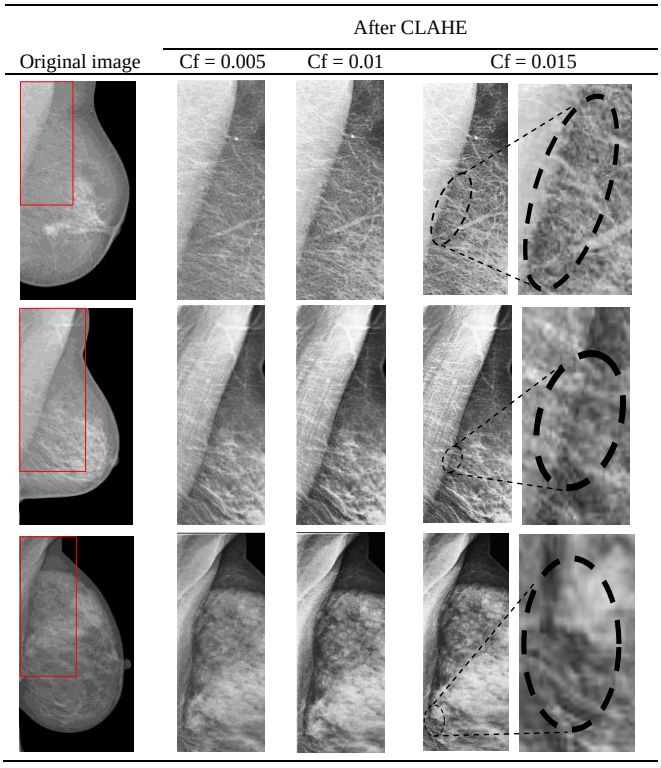

Fig. 3. Enhancement results with three different contrast factors for three different types of breast. Top: a heterogeneously dense breast with convex muscle; Middle: a breast with scattered fibro-glandular tissue and combinatorial muscle; Bottom: a heterogeneously dense breast with combinatorial muscle.

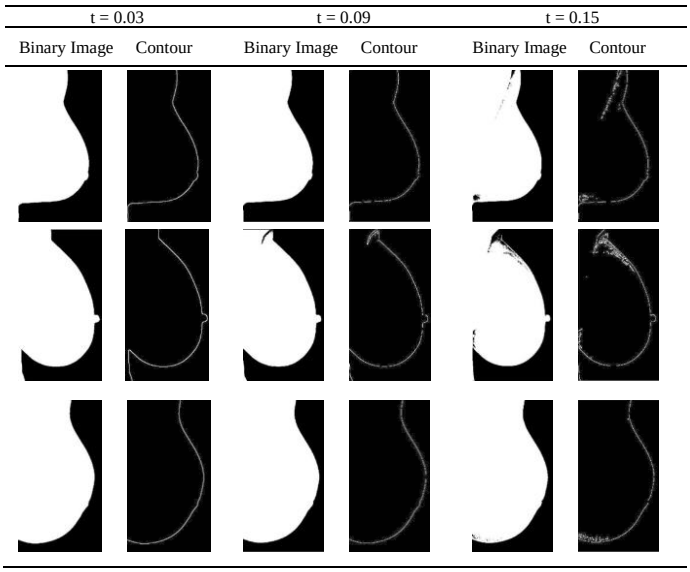

Fig. 4. Testing different values of the contrast factor Cf for three different types of breast. Top: a heterogeneously dense breast with convex muscle; Middle: a breast with scattered fibro-glandular tissue and combinatorial muscle; Bottom: a heterogeneously dense breast with combinatorial muscle.

B. Identification of the muscle location via geometric rules

We now find the maximum inscribed circle (MIC): C_1, within the detected breast contour. Finding the MIC is the first step in geometrically delineating the muscle. We use the method of Xia et al. [22] to find the MIC. This method applies a vector distance transformation strategy to create a distance field, then globally searches the medial axis, radius, and center for the MIC. More details can be found in Xia et al. [22]. The detected breast contour is employed as a mask on the CLAHE image to obtain the MIC. After detecting the MIC process, all subsequent processing is applied on the CLAHE image.

Once the location of the MIC: C_1, with the center (x_O, y_O) and radius r has been specified, the next step in finding the muscle region is to locate the border of the muscle. The border starts from a point we call A. By plotting the mean grey level values of the pixels in the top p rows along the same column of the image we can easily decide point A (Fig. 5). In our experiments, p was tuned empirically being set to 2. Therefore, the second edge (local minimum, or local maximum [33] on a reversed signal) from the right which has a lower (darker) value is the starting location of the pectoral muscle (point A). In the case of a multi-layered muscle, as in the example of Fig. 14(a) second row, if we search for the muscle edge by moving from the left-hand side to the right-hand side of the image, then we might not get the correct edge. However, when we move from the right-hand side to the left (from the dark background towards the breast), the first edge encountered would be the start of the breast tissue, and the second edge would be the edge of the muscle. This method was inspired by the imaging mechanism and the anatomy of the breast and chest. The experiments based on a large number of images in the three publicly accessible datasets show this method is effective.

Thus the method is robust enough to support the multi-

layer muscles (Fig. 14). Because of the anatomy of the breast in the mammograms, the plot of the top 2-4 rows of the mammogram is similar to what we have in Fig. 5.

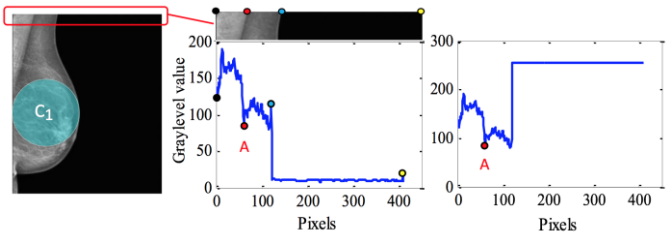

Fig. 5. Finding the MIC in the breast contour (left), masking it on the CLAHE image (middle) and then finding the point A (right) which is the starting location of the pectoral muscle.

Next, we define O as the center of MIC, then calculate the length OA as $OA = ((x_A - x_O)^2 + (y_A - y_O)^2)^{1/2}$. This is shown in Fig. 6(a), where (x_A, y_A) are the coordinates of point A. Once the length of the OA is computed, we draw the tangent line from A to C_1 which is named S.

As can be seen in Fig. 6(b), a right angle triangle is constructed from the line OA, the radius of C_1 and the tangent S. The length of the edge S is computed using $S = ((OA^2) - (r^2))^{1/2}$. We denote the intersection of C_1 and S as D_1. We then plot the circle C_2 centered at A and with the radius of AD_1 shown in Fig. 6(c). The two circles: C_1 and C_2 are defined as C_1: $(x - x_O)^2 + (y - y_O)^2 = r^2$ and C_2: $(x - x_A)^2 + (y - y_A)^2 = (AD_1)^2 = (OA)^2 - r^2$.

As illustrated in Fig. 7, if we extend the line S and denote it as d_1, then the two lines: d_1 and d_2 (the left vertical side of the image) intersect at point B, whose coordinates are computed as follows:

$$\begin{cases} d_1;\ \frac{y-y_A}{x-x_A} = \frac{y_{D1}-y_A}{x_{D1}-x_A} \\ d_2;\ x = 0 \end{cases} \qquad (1)$$

$$x_B = 0,\ \ y_B = -x_A\left(\frac{y_{D1}-y_A}{x_{D1}-x_A}\right) + y_A$$

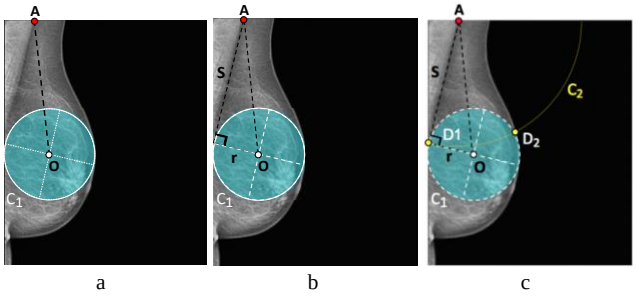

Fig. 6. Finding the location of the border (S) of the pectoral muscle. a) Location of C_1 and line OA, b) Position of the right angle triangle formed by S, AO and radius r. c) Position of the circle C_2 which intersects C_1 at points D_1 and D_2.

Fig. 7 shows the pectoral muscle region enclosed in the triangle *AEB*. As illustrated in Fig. 8, d_1, d_2, and d_3 are three lines forming a right angle triangle, so the pectoral muscle region can be defined by the region contained by them. Formally this is written in Eq. 2, where (x_p, y_p) is any point inside the pectoral muscle region, and d_3 is the upper horizontal side of the image.

$$d_3(x_p, y_p) \le 0\ \&\ d_1(x_p, y_p) \ge 0\ \&\ d_2(x_p, y_p) \le 0 \qquad (2)$$

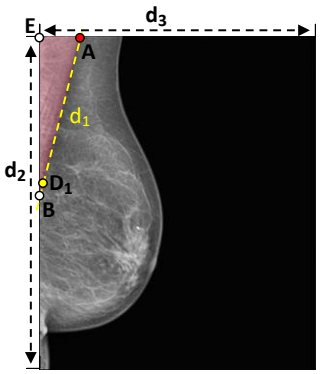

Fig. 7. The pectoral muscle location in an approximating triangle AEB.

C. Optimization of the method for convex and combinatorial muscles

As shown in Fig. 8, the MIC is very helpful for identifying the boundary of the breast efficiently, however the pectoral muscles may be convex, concave or a combination of both. As shown in Fig. 8, in convex pectoral muscles, the muscle region protrudes to the right of line d_1. To overcome the difficulty in segmentation of the irregular shape (curvature) of pectoral muscles, to avoid over-segmentation, and to address the constraint of the straight-line theory imposed by previous methods, we have defined a threshold line d_1* that is plotted parallel to d_1. The threshold line prevents the region growing algorithm from growth beyond d_1*. If we assume the width of the pectoral muscle, EA, is equal to T, then d_1* is defined by shifting the line d_1 to the right by a distance of T/4. The amount of shift (T/4) was obtained experimentally. Therefore, we will have the new triangle: EA'B' for the RG algorithm.

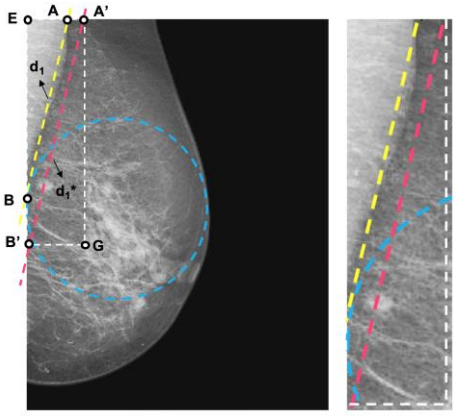

Fig. 8. Specifying the restrictive line d_1* (red dashed-line) at the convex pectoral muscles which avoids over-expansion during the RG algorithm.

In the last step, we optimize our method around d_1* for the RG algorithm [23, 24] which is a luminance region based approach. In most of the recent works, the authors have selected the seed point manually to start the growing but, in this paper, point *A* has been defined as an initial seed point. The algorithm expands the area around *A* to include neighboring pixels that are within a threshold range. The expansion is based on the average intensities of a 15 × 15

region of neighboring pixels to make the algorithm robust against noise. The size of this region was tuned experimentally. The similarity condition we consider uses two thresholds, T_{h1} and T_{h2} [25], given by $T_{h1} = \bar{I} - (0.3 - K).\bar{I}$ and $T_{h2} = \bar{I} - (0.3 + K).\bar{I}$, where $\bar{I}$ is the average value of luminance in the specified region and it is adjusted for every growing step, and K depends on a factor F given by [25],

$$F = \frac{d}{\sqrt{NM}}(I_{max} - I_{seed}) \quad (3)$$

where d is the distance of the pixel with the maximum intensity from point A, I_{seed} is the intensity value of the seed, I_{max} is the maximum intensity value in the expanded area, M is ||EA'||, and N is ||EB'||. Factor F is computed for each ROI and K is set for the best contour. K is related to F by implementing a robust linear regression of the point (K, F). The initial value of K is defined as a + bF, where a and b are determined by the regression model. More details can be found in [24]. Optionally, a radiologist can help tune the parameter K in order to get the best result.

Two main factors that lead to the successful segmentation of the pectoral muscle are the localization of both point A and the line d_1 (or d_1*) which in this paper have been identified accurately (the experimental results validate that the point A and line d_1 have been correctly selected). The expanding area of the region growing algorithm in the convex or combinatorial muscles is from pixel A to the last pixel on the left side of the image and is bound by the threshold line d_1* from the right.

In order to get the best distance for plotting d_1* we tested several different values (see Fig. 9) e.g., T/2 (the blue dashed line), T/4 (the red dashed line), T/6 (the black dashed line), and T/8 (the white dashed line). As can be seen in Fig. 10, in all cases (different tissues, muscle sizes, and breast shapes) the value T/4 properly contains also muscle types placed outside the pectoral muscle line. This is denoted with the color green. The T/6 and T/8 lines sometimes cross the muscle line. Although the T/2 line was also placed outside the muscle, it contains a large portion of the breast which causes higher computational cost and possible inaccurate region growing. Using d_1* to restrict the RG algorithm allows the pectoral muscle to be extracted without affecting other regions of the mammogram images that will be important in the subsequent processing steps. We selected 10 random images from each dataset for determining optimal parameter values (30 images in total). To allow for a fair comparison with other methods in the literature, e.g. [8, 12, 16, and 17], these images were also included when reporting the final results.

An example of convex pectoral muscle segmentation and how the threshold line d_1* provides a boundary for the segmentation is illustrated in Fig. 8. Note that the dashed blue circle is the detected MIC in the breast contour and d_1 is specified according to the previous steps as detailed above. For concave pectoral muscles the d_1* line is not needed and the extraction process can be formulated using only the d_1 line. The process of segmentation of the combinatorial muscles is the same as the convex ones.

The proposed algorithm consists of three main steps: MIC detection, d_1 definition, and d_1* optimization followed by adaptive region growing. The first step involves the whole image for enhancement of the breast contour and MIC detection. The second step detects the starting point A of the pectoral muscle in the top rows in the given image and finds the tangent line d_1 of the MIC through A.

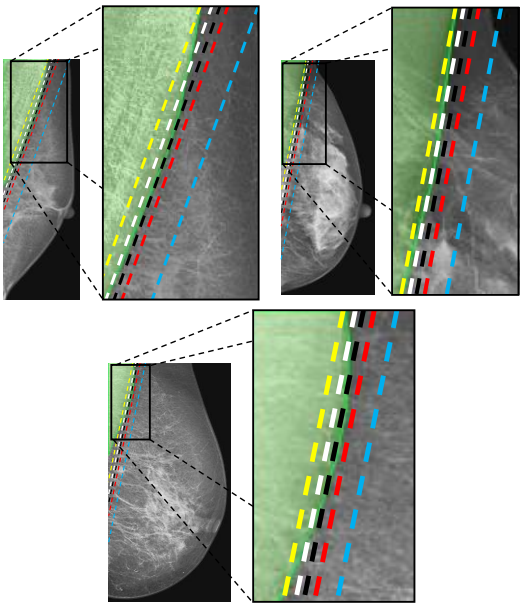

Fig. 9. Different possible values for the restrictive line d_1*.

The third step optimizes the location of the boundary between the breast and the pectoral muscle through translating d_1 to d_1* and adapts the region growing in a small region of the given image. Thus, the proposed method has a linear computational complexity in the number of pixels of the given image.

We proposed further steps after finding line AB to avoid over/under segmentation of the muscle. As shown in Figures 8 and 15 segmenting the muscle using only the direct line AB would cause over/under segmentation. Fitting a polynomial curve or dynamic programing has also been considered for finding the muscle edge. However, polynomial fitting requires the user to decide on the degree of the polynomial function and also requires robustly extracted edge points. Finding the degree may not be simple in practice and may require trial and error as each image is different. Extracting the edge points is also not straightforward given the weak muscle boundary. A dynamic programing approach was also considered as an alternative to a degree-dependent polynomial, but again, as the intensity transition across the boundary of dense breasts is not clear, the user would have to ensure a suitable energy function with at least two terms (data and regularization terms) and decide on a proper weight that balances these terms or resort to inserting seed points manually along the boundary (as is common with the dynamic-programming based live-wire method [35]).

III. Results and Discussion

Similar to several other works in the literature [16, 36, 37],

one radiologist assessed the results visually. Segmentation quality was validated through visual inspection by the radiologist and by quantitatively comparing the extracted regions with hand drawn contours (ground truth) after contrast enhancement.

To quantitatively evaluate the performance of the proposed segmentation algorithm, the Jaccard index [26] and Dice similarity coefficient [27] have been calculated which are defined as:

$$Jaccard = \frac{\left|R_a^i \cap R_m^i\right|}{\left|R_a^i \cup R_m^i\right|} \quad (4), \qquad Dice = \frac{2\left|R_a^i \cap R_m^i\right|}{\left|R_a^i\right| + \left|R_m^i\right|} \quad (5)$$

Where R_a^i and R_m^i are the pixels of the *i*th tissue type segmented by the proposed automatic method and the manual method respectively. The Jaccard and Dice metrics take values between 0 and 1: zero is obtained when two sets have no common elements while one is achieved when two sets are identical. The larger the values the more accurate the segmentation. In addition to reporting the Jaccard index and the Dice similarity coefficient, we also calculate the distances between the ground truth delineation and the boundary of the automatic segmentation. Given that for every point on one contour (i.e. the automatic segmentation) there is a minimum distance to the other contour (i.e. the ground truth), we report the, max (a.k.a. Hausdorff), and the mean of these inter-contour minimum distances.

The proposed method has been applied to MLO images randomly selected from three datasets of INbreast [28] (197 images), IRMA (Image Retrieval in Medical Applications) a version of DDSM [29] (353 images), and The Mammographic Image Analysis Society (MIAS) [30] (322 images). We would like to emphasize that modern digital mammography systems produce clearer images (INbreast) than traditional systems that digitize the images using scanners (MIAS, DDSM). There are no artifacts and textual labels on images captured by modern mammographic imaging systems. In order to compare the proposed method with previous methods we also included the older MIAS and DDSM datasets. Radiopaque artifacts and labels which are shown in Fig. 10 (a) may produce an error in detecting the breast contour. We can easily remove them by running a simple morphological operation introduced by Nagi et al. [31]. A sample mammogram image, with the radiopaque artifacts suppressed has been demonstrated in Fig.10 (c).

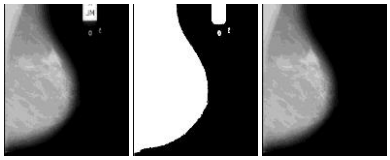

a b c

Fig. 10. A sample image in the MIAS dataset with Radiopaque artifacts removed; a) original image, b) binary image, c) image with artifacts removed

The average similarity measure of Jaccard and Dice indices between the regions segmented by the proposed geometric method and ground truth are plotted in Fig. 11. The 'NRM', 'CVX', 'CCV', and 'CMB' are abbreviations of normal, convex, concave, and combinatorial. The thin black lines in the middle of the bars show the standard deviation. The results indicate that the proposed algorithm is promising in pectoral muscle segmentation for all four BI-RADS density classes. Note that the two datasets of INbreast and DDSM are based on four BI-RADS tissue density classes of almost entirely fatty (1), scattered fibro glandular (2), heterogeneously dense (3), and extremely dense (4) while the MIAS data is based on the three tissue density classes of fatty (F), fatty-glandular (Fg), and dense-glandular (Dg).

The majority of the data for testing the algorithm is from classes 2 and 3 of the BI-RADS density classes because most women are included in these two classes (about 80%) [32]. As can be seen from Fig. 11, strong results have been achieved by the proposed segmentation algorithm for these two classes (2&3). For the class 2 density of the INbreast data, the Jaccard and Dice metrics were 0.976±0.013 and 0.987±0.006 respectively. For class 3, the Jaccard and Dice metrics were 0.972±0.008 and 0.986±0.004 respectively. For the class 2 density of the DDSM data the Jaccard and Dice metrics were 0.972±0.013 and 0.986±0.007, respectively. For class 3 the Jaccard and Dice metrics were 0.964±0.006 and 0.982±0.003 respectively. For the class Fg of the MIAS data the Jaccard and Dice metrics were 0.976±0.013 and 0.987±0.006 respectively. For the class Dg, Jaccard and Dice indices were 0.973±0.009 and 0.986±0.005 respectively. The most difficult category is the extremely dense breasts. Recent papers have not explicitly mentioned results of their segmentation. For this class our method achieved Jaccard and Dice indices of 0.960±0.01 and 0.978±0.008 respectively.

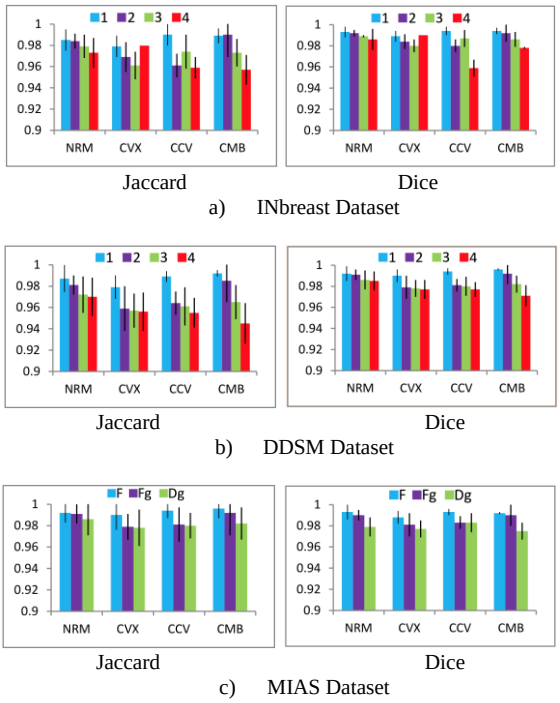

Fig. 11. Averages and standard deviations of Jaccard and Dice indices of pectoral muscle segmentation of the proposed method results for the INbreast, DDSM, and MIAS datasets.

The Hausdorff and mean distances between the contours detected by our proposed method and the ground truth is presented in Fig. 12. We achieve, on average, sub-millimeter accuracy on all datasets. The Hausdorff distance captures the accuracy of the worst localized regions of the muscle boundary, yet this remains below 1 cm. Fig. 13 (a) shows a heterogeneously dense breast. The area marked by a dashed red oval is where the RG algorithm produces an error because there is no clear border between the muscle and breast tissue. This type of error is common in heterogeneously and extremely dense breasts. The yellow and yellow dashed lines in Fig. 13 (b) are the d_1 and d_1* lines respectively.

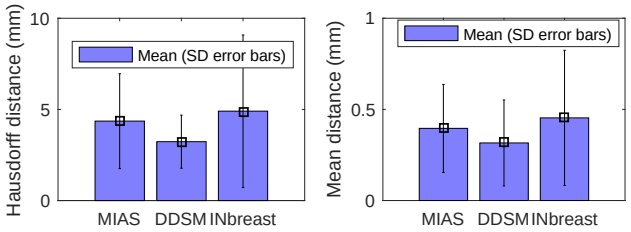

Fig. 12. The Hausdorff (left) and mean (right) distance results of the muscle segmentation using the proposed method.

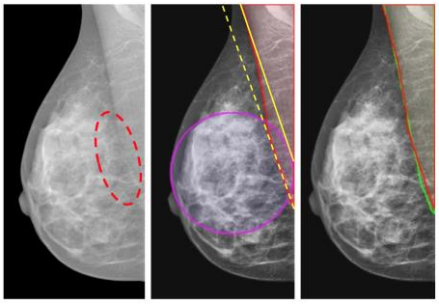

Fig. 13. An example muscle segmentation for a heterogeneously dense breast, a) Error producing region circled in red, b) The limitation boundary d_1* shown as the yellow dashed line, which solves this problem, c) The region identified by the proposed algorithm (red) and GT (green).

As can be seen, the d_1* line limited the possible region for the RG algorithm for accurate segmentation results illustrated in Fig. 13 (c). All the muscles are considered as convex/combinatorial. Therefore, we always draw line d_1* and run the RG method. Fig. 14 shows the output of using the two lines d_1 and d_1* + RG method. As mentioned above, the most important category of density class is the extremely dense class that contains more than 75% glandular and fibrous tissue because it is involved with a high risk of cancer. A sample result from this class with an acceptable segmentation can be seen in Fig. 14. In contrast, it is unclear how the previous methods in the literature would work for this class. The methods based on region growing or clustering will produce significant errors in these cases due to the similarity in appearance and complex geometry of the muscle and breast tissue. Another limitation of some of the methods reviewed in the literature is that they have not shown how accurately they deal with multi-layer muscles. Our method achieved considerably high accuracy as illustrated in Fig. 14 (an extremely dense breast with multi-layer pectoral muscle). Note that these images are much harder to analyze than other multi-layer images because in addition to being multi-layer they represent extremely dense breasts. Nevertheless, our method accurately segmented the pectoral muscle.

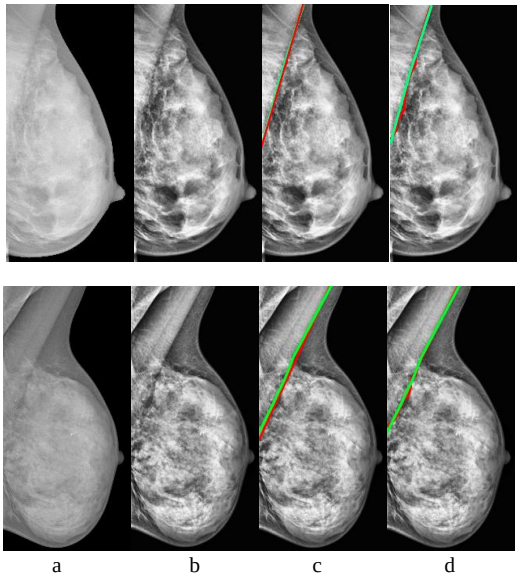

Fig. 14. Sample results of the proposed segmentation method (red) compared with the ground truth (green). a) Original image, b) CLAHE image, c) Ground truth vs. line d_1, d) Ground truth vs. segmented region using d_1* and RG. The first row is an extremely dense breast and the second row is a breast with a multilayered muscle.

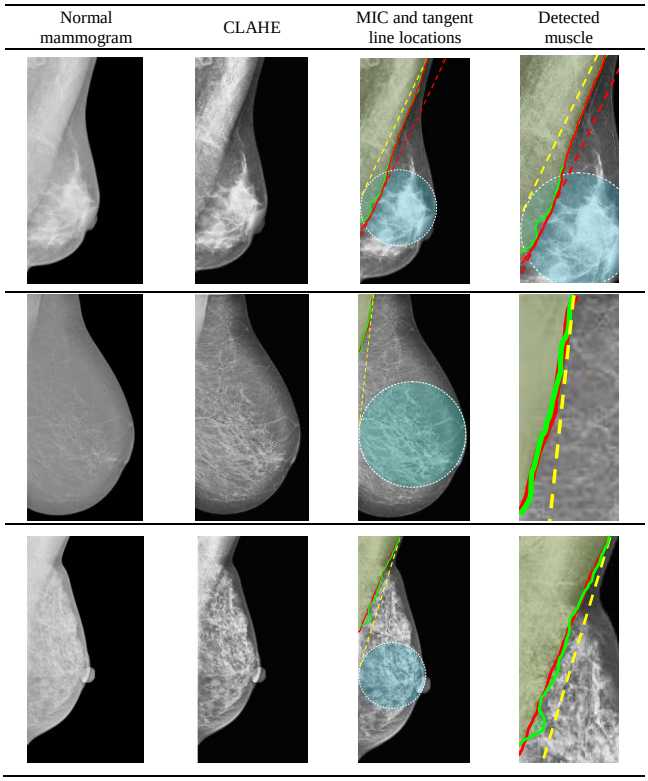

Fig. 15. Three samples of different breast types and their pectoral muscle segmentation results. The MIC is denoted by a blue circle, the ground truth is given by the green region and our results are given by the red region. Additionally, the yellow dashed line shows the limitation boundary.

Mammograms have a very similar structure, but the location, size, and shape of the breasts vary. As three samples of Fig. 15 show, a mammogram could be taken in such a way that the biggest portion of the breast might not coincide with the location where the pectoral muscle starts. Nonetheless, the proposed method effectively handles these cases. Fig. 16 shows the failed, successful, and acceptable segmentation results, respectively. The red area is the region identified by our automatic algorithm, and the green region is the ground truth (GT). As shown in Fig. 16(a), the presence of the arm in the image caused an error. It should be noted that this situation rarely occurs as the images are captured using a standard procedure and device. However, these cases are easily screened out by the clinician and should not lead to a misdiagnosis. Fig. 16(c) shows an example of acceptable concave pectoral muscle identification.

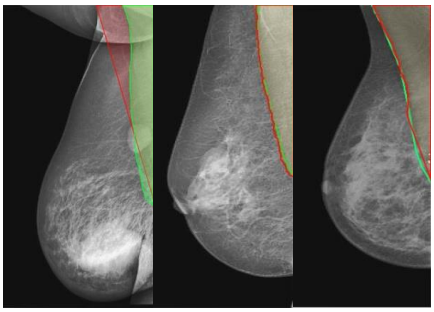

Fig. 16. Sample results of the proposed segmentation method (red) compared with the ground truth (green). a) an unacceptable result, b) an accurate result, c) an acceptable result.

As was shown qualitatively in Figures 13-15, and demonstrated quantitatively in Fig. 11, our method was largely successful in segmenting a variety of cases and muscle types (breasts with different sizes/shapes/tissue densities; muscles with various shapes: multilayer, concave, convex, and combinatorial) and outperforming state-of-the-art. Nevertheless, there were different failure cases due to two main reasons: (i) The presence of the patient's arm, which changed the profile of the intensities of the pixels in the image, and (ii) the weak boundaries between the pectoral muscle and breast tissue causing an ambiguity in determining the muscle borders. Figures 16 (a) and 17 show 4 example failure cases.

Figures 17(i) and 17(ii) show two failed cases caused by the presence of a part of the patient's arm within the field of view, which resulted in multiple intensity transitions between the pectoral muscle and the breast and, hence, the ambiguity in determining their borders. Fig. 17(iii) shows another case in which the border of the muscle and the breast tissue is not clear in the original image. This has prevented the proposed method from excluding the muscle region from the breast tissue. Even so, the result is still acceptable. The small red arrows in Fig. 17(iii), show the area where the muscle edge is mixed with the breast tissue making the muscle border identification difficult. These cases are challenging to delineate even by experts.

As shown above, the proposed method is robust enough to handle contrast variation, intensity variation, edge size variation, multi-layered muscles, and the curvature of the muscle boundary. The proposed geometric rule based method shows superior results on the extremely dense breast in addition to the other density classes. In order to compare with other methods a five-point assessment scale (Table 1), introduced by Kwok et al. [12] was adopted.

TABLE I
DESCRIPTION OF FIVE-POINT ASSESSMENT SCALE

Assessment scale	Notation	Description
Exact	E	The detected borders fit the ground truth exactly and there is not any visual deviation.
Optimal	O	The detected region specifies the muscle region exactly for at least half of its length and adequately for the remaining part.
Adequate	A	The detected region specifies the muscle margin exactly, but with acceptable accuracy for specific purpose.
Sub-optimal	S	The identified region is not adequate for at least half of its length.
Inadequate	I	The segmented region is so inacceptable as to be inadequate for the intended purpose.

The performance of the proposed method based on a radiologist's opinion has been illustrated in Fig. 18. The 'E',

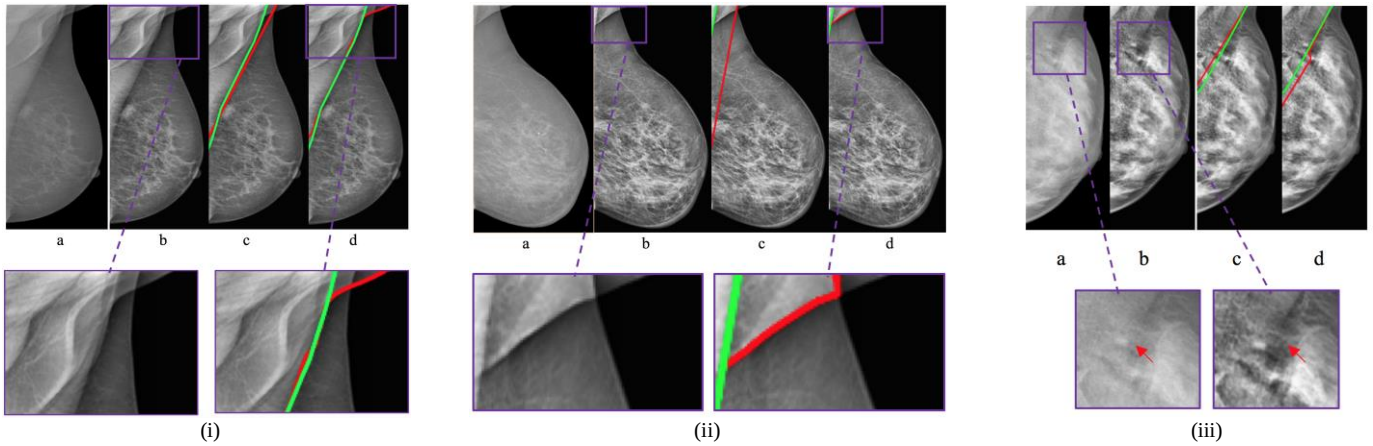

Fig. 17. Sample failure results of the proposed segmentation method (red) compared with the ground truth (green). a) Original image, b) CLAHE image, c) Ground truth vs. line d_1, d) Ground truth vs. segmented region using d_1* and RG.

'O', and 'A' have been grouped as acceptable results while 'S' and 'I' are classified as unacceptable results.

Our method achieved strong segmentation results with rates of 96%, 94%, and 95% for the MLO views of the INbreast, DDSM, and MIAS datasets respectively with a low unacceptable rate. We have no segmentation results in the group of 'I' for any of the three datasets. We compared our results with three other methods because the same assessment criterion was applied. The comparison results are shown in Table 2. In comparison to other previous methods the proposed method had a superior performance based on the number of acceptable results (E+O+A).

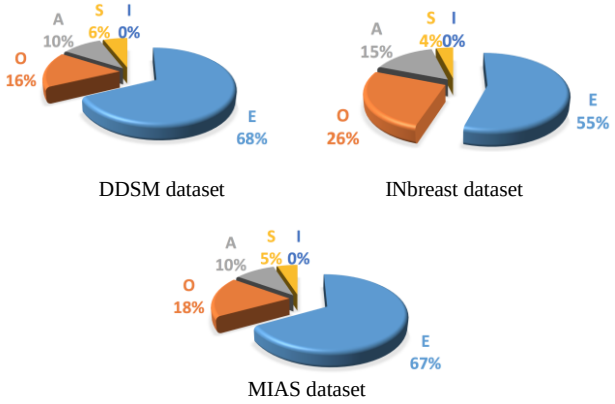

Fig. 18. Visual assessment of the results by radiologists for different datasets

As can be seen in Table 2, Kwok's method has an accuracy of 83.9%. It is precise for a straight-line segment pectoral muscle edge, but the performance degrades significantly in cases where the mammograms' pectoral muscle border curves away from the chest wall. In contrast, our method applies the threshold line to solve this defect. Wang et al., tried to solve the curvature limitations of the muscle and they obtained an accuracy of 91%. However, their method is strongly dependent on the image contrast, while we propose to use the adaptive RG method to handle this issue. In other competitive work, Li et al. had a slightly improved accuracy (90.06%~92%). Their method is based on intensity deviation. The basic steps of our method are made by geometric rules and adaptive region growing which are robust to intensity or contrast change in mammograms, hence the improved performance of the segmentation.

IV. Conclusion

This paper has proposed a novel geometry based pectoral muscle segmentation method. This method takes advantages of geometric rules automatically and finds the starting point of the pectoral muscle and maximum inscribed circle in the breast contour. This allows the muscle borders to be identified. A threshold line and region growing were proposed to optimize the method performance on convex, concave, and combinatorial muscles. The method was tested on 872 MLO images and achieved strong results on all BI-RADS tissue density classes, especially extremely dense breasts, whose segmentation results are missing in the literature. The proposed method has the potential to be used in computer aided diagnosis systems as a preprocessing step. Our experimental results also indicate that the proposed algorithm is versatile enough to be applied to extensive varieties in the appearance of the pectoral muscle; it remains successful when superimposed breast tissue occludes the pectoral muscle edge.

While the accuracy achieved by our method is high (>90%) and outperformed competing methods, there are still cases that would benefit from user interaction for an improved segmentation. Future work, towards CADx systems should assess the effect of such errors on the segmentation on the final diagnosis task. In order to improve the segmentation accuracy, possibilities for future work include: Exploring optimization-based segmentation techniques (instead of region growing) [25]; searching the hyper-parameters space using rigorous methods (instead of using the method proposed by Menchattini et al. [25] for setting the region growing thresholds, or for setting the CLAHE method parameters), e.g. via harmony search [43] and evolutionary computing [44] or combinatorial/continuous optimization of hyper-parameters [39-41]; or setting hyper-parameter values based on image contents [42]. However, it remains to be seen whether such additional methodological complexity will lead to worthwhile improvements in accuracy. Another potential future research direction is to investigate direct (or segmentation-free) methods [38] that predict disease classes without even resorting to segmentation-based feature extraction.

TABLE II
Description of Five-Point Assessment Scale

Reference	Methodology	Database	No. of Images	Acceptable Results
Kwok et al. [12]	Straight line estimation and cliff detection	MIAS	322	83.9%
Wang et al. [17]	Markov chain and active contour model	DDSM	200	91%
Mustra et al. [16]	bit depth reduction and wavelet decomposition	Private	40	85%
Li et al. [8]	Homogenous texture and intensity deviation based method	DDSM	100	92%
		MIAS	322	90.06%
Proposed method	Geometry based model	DDSM	353	**94%**
		MIAS	322 (4 images have no pectoral muscle)	**95%**
		INbreast	197	**96%**

ACKNOWLEDGMENT

The authors would like to thank the Breast Research Group, INESC Porto, Portugal and Prof. TM Deserno, Dept. of Medical Informatics, RWTH Aachen, Germany for providing the two data-sets of INbreast and IRMA version of DDSM respectively.

REFERENCES

[1] World-Health-Organization (2013). Cancer, WHO, Fact sheet N°297. World Health Organization (ed).

[2] M.L. Giger, N. Karssemeijer, S. G. A. III. (2001). Computer-aided diagnosis in medical imaging. *Medical Imaging, IEEE Transaction on*. 20(12), pp. 1205-1208.

[3] M. Elter, A. Horsch (2009). CADx of mammographic masses and clustered microcalcifications: a review. *Medical physics*. 36(6), pp.2052-2068.

[4] K. Ganesan, U.R. Acharya, K.C. Chua, L.C. Min, K.T. Abraham (2013). Pectoral muscle segmentation: A review. *Computer Methods and Programs in Biomedicine*. 110(1), pp. 48-57.

[5] F.C. Ghesu, M. Wels, A. Jerebko, M. Sühling, J. Hornegger, B.M. Kelm (2014). Pectoral Muscle Detection in Digital Breast Tomosynthesis and Mammography. *Medical Computer Vision, Third International MICCAI Workshop, Large Data in Medical Imaging (Springer)*. 8331, pp.148-157.

[6] L. Liu, Q. Liu, W. Lu (2014). Pectoral Muscle Detection in Mammograms Using Local Statistical Features. *Journal of digital imaging*. 27(5), pp. 633-641.

[7] X. Chen, E. Moschidis, C. Taylor, S. Astley (2014). A Novel Framework for Fat, Glandular Tissue, Pectoral Muscle and Nipple Segmentation in Full Field Digital Mammograms. *Breast Imaging (Springer)*. 8539, pp. 201-208.

[8] Y. Li, H. Chen, Y. Yang, N. Yang (2013). Pectoral muscle segmentation in mammograms based on homogenous texture and intensity deviation. *Pattern Recognition*. 46(3), pp. 681-691.

[9] M. Mustra, M. Grgic (2013). Robust automatic breast and pectoral muscle segmentation from scanned mammograms. *Signal Processing*, 93(10), pp. 2817-2827.

[10] C. Balleyguier, S. Ayadi, K. Van Nguyen, D. Vanel, C. Dromain, R. Sigal (2007) BIRADS™ classification in mammography. *European journal of radiology*. 6(2), pp. 192-194.

[11] I. K. Maitra, S. Nag, S.K. Bandyopadhyay (2012). Technique for preprocessing of digital mammogram. *Computer Methods and Programs in Biomedicine*. 107(2), pp. 175-188.

[12] S. M. Kwok, R. Chandrasekhar, Y. Attikiouzel, M.T. Rickard (2004). Automatic pectoral muscle segmentation on mediolateral oblique view mammograms. *Medical Imaging, IEEE Transactions on*. 23(9), pp. 1129-1140.

[13] R. J. Ferrari, R. M. Rangayyan, J.L. Desautels, R. Borges, A. F. Frere (2004). Automatic identification of the pectoral muscle in mammograms. *Medical Imaging, IEEE Transactions on*. 23(2), pp. 232-245.

[14] F. Ma, M. Bajger, J. P. Slavotinek, M. J. Bottema(2007). Two graph theory based methods for identifying the pectoral muscle in mammograms. *Pattern Recognition*. 40(9), pp. 2592-2602.

[15] D. Raba, A. Oliver, J. Martí, M. Peracaula, J. Espunya (2005). Breast segmentation with pectoral muscle suppression on digital mammograms. *Pattern Recognition and Image Analysis (Springer)*. 3523, pp. 471-478.

[16] M. Mustra, J. Bozek, M. Grgic (2009). Breast border extraction and pectoral muscle detection using wavelet decomposition. *EUROCON 2009, EUROCON '09. IEEE, St.-Petersburg*, pp. 1426-1433.

[17] L. Wang, M.-l. Zhu, L.-p. Deng, X. Yuan (2010). Automatic pectoral muscle boundary detection in mammograms based on Markov chain and active contour model. *Journal of Zhejiang University SCIENCE C*. 11(2), pp. 111-118.

[18] K. S. Camilus, V. Govindan, P. Sathidevi (2010). Computer-aided identification of the pectoral muscle in digitized mammogram. *Journal of digital imaging*. 23(5), pp. 562-580.

[19] K.S. Camilus, V. Govindan, P. Sathidevi (2011). Pectoral muscle identification in mammograms. *Journal of Applied Clinical Medical Physics*.12(3), pp.215-230.

[20] N. F. Boyd, H. Guo, L. J. Martin, L. Sun, J. Stone, E. Fishell, R. A. Jong, G. Hislop, A. Chiarelli, S. Minkin (2007). Mammographic density and the risk and detection of breast cancer. *New England Journal of Medicine*. 356(3) pp. 227-236.

[21] M. T. Mandelson, N. Oestreicher, P. L. Porter, D. White, C. A. Finder, S. H. Taplin, E. White (2000). Breast density as a predictor of mammographic detection: comparison of interval-and screen-detected cancers. *Journal of the National Cancer Institute*. 92(13), pp. 1081-1087.

[22] R. Xia, W. Liu, J. Zhao, H. Bian, F. Xing (2007). Robust Algorithm for Detecting the Maximum Inscribed Circle. *Computer-Aided Design and Computer Graphics, 10th IEEE International Conference on*, pp. 230-233.

[23] G. Rabottino, A. Mencattini, M. Salmeri, F. Caselli, R. Lojacono (2008). Mass contour extraction in mammographic images for breast cancer identification. *16th IMEKO TC4 Symposium, Exploring New Frontiers of Instrumentation and Methods for Electrical and Electronic Measurements*, Florence. Italy.

[24] A. Mencattini, G. Rabottino, M. Salmeri, R. Lojacono, E. Colini (2008). Breast mass segmentation in mammographic images by an effective region growing algorithm. *Advanced Concepts for Intelligent Vision Systems (Springer)*. 5259, pp. 948-957.

[25] A. Mencattini, M. Salmeri, G. Rabottino, S. Salicone (2010). Metrological characterization of a CADx system for the classification of breast masses in mammograms. *Instrumentation and Measurement, IEEE Transactions on*. 59(11), pp. 2792-2799.

[26] P. Jaccard (1912). The distribution of the flora in the alpine zone", *New phytologist*. 11(2), pp. 37-50.

[27] L.R. Dice (1945). Measures of the amount of ecologic association between species. *Ecology*. 26(3), pp. 297-302.

[28] I.C. Moreira, I. Amaral, I. Domingues, A. Cardoso, M.J. Cardoso, J.S. Cardoso (2012). INbreast: Toward a full-field digital mammographic database. *Academic Radiology*.19(2), pp. 236-248.

[29] J.E. De Oliveira, A.M. Machado, G.C. Chavez, A.P.B. Lopes, T.M. Deserno, A.d.A. Araújo (2010). MammoSys: A content-based image retrieval system using breast density patterns. *Computer Methods and Programs in Biomedicine*. 99(3), pp. 289-29.

[30] J. Suckling, J. Parker, D. Dance, S. Astley, I. Hutt, C. Boggis, I. Ricketts, E. Stamatakis, N. Cerneaz, S.-L. Kok (1994). The mammographic image analysis society digital mammogram database.

[31] J. Nagi, S. Abdul Kareem, F. Nagi, S.K. Ahme (2010). Automated breast profile segmentation for ROI detection using digital mammograms. *Biomedical Engineering and Sciences (IECBES), IEEE EMBS Conference on*. pp. 87-92.

[32] Alaska Regional Hospital, Imaging & Radiology, Breast density (2013): http://alaskaregional.com/service/info/breast-density. Accessed: 2016-07-30.

[33] Liutkus, A (2015). Scale-Space Peak Picking. *Inria Nancy-Grand Est (Villers-l`es-Nancy, France)*.

[34] Wei-Ying Ma; Manjunath, B.S. (2000). EdgeFlow: a technique for boundary detection and image segmentation. *Image Processing, IEEE Transactions on*. 9(8), pp. 1375-1388.

[35] Mortensen, Eric N., and William A. Barrett (1998). Interactive segmentation with intelligent scissors. *Graphical models and image processing*. pp. 349-384.

[36] Kwok, S. M., R. Chandrasekhar, and Y. Attikiouzel (2001). Automatic pectoral muscle segmentation on mammograms by straight line estimation and cliff detection. *In Intelligent Information Systems Conference, IEEE, The Seventh Australian and New Zealand*. pp. 67-72.

[37] Chakraborty, Jayasree, Sudipta Mukhopadhyay, Veenu Singla, Niranjan Khandelwal, and Pinakpani Bhattacharyya (2012). Automatic detection of pectoral muscle using average gradient and shape based feature. *Journal of digital imaging*. 25(3), 387-399.

[38] Zhen, Xiantong, and Shuo Li (2015). Towards Direct Medical Image Analysis without Segmentation. *arXiv preprint arXiv:1510.06375*.

[39] M. Szummer, P. Kohli, and D. Hoiem (2008). Learning CRFs using graph cuts. *In Proceedings of the 10th European Conference on Computer Vision*. pp. 582–595.

[40] Chris McIntosh and Ghassan Hamarneh (2009). Optimal Weights for Convex Functionals in Medical Image Segmentation." *In International Symposium on Visual Computing: Special Track on Optimization for Vision, Graphics and Medical Imaging: Theory and Applications (ISVC OVGMI)*. 5875-I, pp. 1079-1088.

[41] Chris McIntosh and Ghassan Hamarneh (2007). Is a Single Energy Functional Sufficient? Adaptive Energy Functionals and Automatic

Initialization. *In Lecture Notes in Computer Science, Medical Image Computing and Computer-Assisted Intervention (MICCAI).* 4792, pp. 503-510.

[42] J. Rao, R. Abugharbieh, and G. Hamarneh (2010). Adaptive regularization for image segmentation using local image curvature cues. *In European Conference on Computer Vision (ECCV)*.

[43] Z.W. Geem, J.H. Kim, and G. V. Loganathan (2001). A new heuristic optimization algorithm: harmony search. *Simulation*. 76(2), pp. 60-68.

[44] D. Goldberg (1989). Genetic Algorithms in Search, Optimization and Machine Learning. *Reading, MA: Addison-Wesley Professional*, ISBN 978-0201157673.